Duration of Individual Relativistic Electron Microbursts: A Probe Into Their Scattering Mechanism

M. Shumko[1,2], L.W. Blum[3], and A.B. Crew[4]

[1]NASA's Goddard Space Flight Center, Greenbelt, Maryland, USA
[3]Universities Space Research Association, Columbia, Maryland, USA
[3]University of Colorado Boulder, Boulder, Colorado, USA
[2]Johns Hopkins University Applied Physics Laboratory, Laurel, Maryland, USA

Key Points:

- We identified relativistic microbursts observed by the SAMPEX satellite and quantified their duration
- The microburst duration interquartile range is 70-140 ms and shows trends in AE, L-shell, and MLT
- Microburst durations are shortest at midnight and longest at noon MLT, showing a similar trend to chorus element durations.

Corresponding author: M. Shumko, `msshumko@gmail.com`

Abstract

In this study we used the Solar Anomalous and Magnetospheric Particle Explorer to identify and quantify the duration of > 1 MeV electron microbursts. We investigated the microburst duration trends as a function of geomagnetic activity, L-shell, and magnetic local time (MLT)—with the most evident duration trend in MLT. The shortest microbursts, with a median duration around 80 milliseconds, were observed near midnight MLT. Microburst duration increases from midnight and noon MLT, where at noon the median microburst duration doubles to 160 milliseconds. The increasing microburst duration trend in MLT is similar to the whistler mode chorus rising tone element duration, shedding light into the microburst scattering mechanism.

Plain Language Summary

Finish this section. Microbursts are a naturally occurring form of electron precipitation from near-Earth space into the atmosphere. They are characterized by their short duration, often assumed to be less than a second. Microburst impact on the atmosphere includes the degradation of Mesospheric Ozone through the production of Odd Nitrogen and Odd Hydrogen molecules... We don't know the details on how microburst electrons are scattered, but there is evidence that they are scattered by whistler-mode chorus rising tone elements... Talk about duration and how it is a probe into the scattering physics.

1 Introduction

Earth's outer radiation belt electron population is in constant flux, governed by many processes that affect charged particles via, for example: radial transport with injections from the magnetotail and ultra low frequency waves, local heating and loss into Earth's atmosphere due to wave-particle interactions Cite Ripoll et al., 2019 "Particle Dynamics in the Earth's Radiation Belts: Review of Current Research and Open Questions". Whistler mode chorus (WMC) is just one type of plasma wave characterized by short (≈ 100 ms) rising tone elements, and perform a dual role in electron dynamics: accelerating electrons from 10s keV to MeV energies, as well as pitch angle scattering electrons into the atmosphere (e.g. Li, Thorne, Angelopoulos, Bonnell, et al., 2009; Thorne, 2010; Horne & Thorne, 2003; Summers, 2005). One form of electron precipitation are microbursts: a transient and intense increase of electrons, with a < 1 second duration. Microbursts were first observed by balloons in Earth's upper atmosphere, and later by satellites in low Earth orbit (LEO), and recently at high altitude near the magnetic equator (e.g. Anderson & Milton, 1964; Blake et al., 1996; Lorentzen et al., 2001; O'Brien et al., 2003; Douma et al., 2017; Kurita et al., 2016; Shumko et al., 2018).

Microburst electron energies span multiple orders of magnitude from tens of keV observed by, for example, Datta et al. (1997); to > 1 MeV observed by the Solar Anomalous Magnetospheric Particle Explorer (SAMPEX) by Blum et al. (2015). Microbursts are predominately observed outside the plasmapause on the radiation belt footprints, $L \approx 4 - 8$, and in the midnight to morning Magnetic Local Times (MLT) ($\approx 0 - 12$ hours MLT) (Lorentzen et al., 2001; Blum et al., 2015; O'Brien et al., 2003; Douma et al., 2017). While microbursts are observed under all geomagnetic conditions, Douma et al. (2017) showed that microburst frequency dramatically increases with the Auroral Electrojet (AE) index, and O'Brien et al. (2003) showed a similar trend with the microburst frequency with the Disturbance storm time index.

The relative impact of microbursts on the ionization of Earth's atmosphere and the depletion of radiation belt electrons is uncertain cite Kathy's paper once it shows up online, but the impact of microbursts alone is estimated to be substantial. Microbursts can deplete the outer radiation belt electrons in as little as a few hours, and can deplete up

to 20% of upper mesospheric ozone (O'Brien et al., 2004; Thorne et al., 2005; Douma et al., 2019; Breneman et al., 2017; Seppälä et al., 2018).

Electron microbursts are widely believed to be scattered by chorus waves. They were associated early on, due to the similar duration of microbursts and chorus rising tone elements, and a similar occurrence distributions in MLT (e.g. Lorentzen et al., 2001). Breneman et al. (2017) directly linked a chorus rising tone element to a microburst observed by the Focused Investigation of Relativistic Electron Bursts: Intensity, Range, and Dynamics CubeSats (FIREBIRD-II; Crew et al. (2016); Johnson et al. (2020)) during a close magnetic conjunction. With this evidence, the particle precipitation community is largely in agreement that chorus waves scatter microbursts.

A natural follow-on question is how. For example, it is still unclear if relativistic (> 1 MeV) microbursts are scattered via cyclotron resonance at high magnetic latitudes, or a higher resonance harmonic near the magnetic equator (Lorentzen et al., 2001). One way to address this question is by studying for how long microburst electrons are in resonance with a chorus wave. The resulting microburst duration, i.e. the microburst width in the time series data, is a probe into the conditions necessary to scatter microburst electrons. From our literature review, we found only qualitative estimates of the microburst duration. Therefore, we used the microbursts observed by the SAMPEX satellite to quantify the distribution of > 1 MeV microburst duration. In this letter, we quantify the duration distribution of microbursts as a function of L-shell, MLT, and the Auroral Electrojet. We then compare these results to prior chorus rising tone element studies, and a chorus-electron scattering model.

2 Instrumentation

In this study we used the > 1 MeV electron count data, taken by the Heavy Ion Large Telescope (HILT) instrument (Klecker et al., 1993), that was onboard the SAMPEX satellite (Baker et al., 1993).

SAMPEX was launched in July 1992 and reentered Earth's atmosphere in November 2012. It was in a 520x670 km, 82° inclination low Earth orbit. In general, the SAMPEX had two pointing modes: spin and orbit rate rotation (zenith pointing) modes. To avoid the compounding effects due to the variable pitch angles sampled in the spin mode, we only used the zenith pointing mode data. The International Geomagnetic Reference Field (Thébault et al., 2015, IGRF) magnetic field model was used to derive the meomagnetic coordinates.

We used the HILT electron data, sampled at a 20 ms cadence (state4 in the data archive), that was taken between 1997 and 2012. The HILT instrument consisted of a large rectangular chamber with the aperture on one end, and 16 solid state detectors on the other. The electron counts accumulated over 20 ms were summed from all of the solid state detectors and used in this study.

The HILT instrument is ideal for studying relativistic microbursts and it was used in many prior microburst studies including O'Brien et al. (2003); Lorentzen et al. (2001); Blake et al. (1996); Nakamura et al. (2000); Kurita et al. (2016), and Douma et al. (2017).

3 Methodology

To estimate the microburst duration we first identified microbursts and then we fit them with a Gaussian model with a linear trend to quantify the duration for each microburst.

Figure 1. Examples > 1 MeV microbursts are shown by the black lines, and the fits are shown by the dashed red lines. The fit full width at half maximum (FWHM) and the $\bar{R}^2$ goodness of fit metric is annotated in each panel. Microbursts with $\bar{R}^2 > 0.9$ were used for this study. The major time ticks are at every second, while the minor ticks are at every 100 milliseconds.

3.1 Microburst Identification

We identified microbursts using the burst parameter defined by O'Brien et al. (2003) and used in numerous other microburst studies with SAMPEX (e.g. Douma et al., 2017). Assuming Poisson probability for the observed electron counts, the burst parameter is the number of standard deviations of a foreground signal above the background, expressed as

$$n_\sigma = \frac{N - A}{\sqrt{A + 1}} \tag{1}$$

where N is the number of foreground electron counts (microburst or otherwise), and A is the centered running average background counts. The 1 in the denominator prevents a division by 0 error. In O'Brien et al. (2003), and in the results in this study, N was summed over 0.1 seconds and is called N_{100}, while A was summed over 0.5 seconds and is called A_{500}. Henceforth we will specify the time window with the subscript for N and A. Times when $n_\sigma > 10$ are classified as microburst times, and the peak count rate in each time interval is saved as a microburst to our data set. With A_{500} and N_{100}, we detected a total of 256,764 microbursts over the 15 year period from 1997 to 2012. Four examples of microbursts are shown in Fig. 1 by the solid black curves.

Check the argument for clarity The choice of A determines the sensitivity of the burst parameter to microbursts of various durations (widths). This sensitivity is best illustrated with an example. Given a hypothetical 1-second wide microburst, if we use A_{500}, the centered average background spanning the microburst time shifts up in counts towards the microburst peak and thus n_σ is reduced, potentially below the detection threshold. On the other hand, if we use A_{1000}, the centered running background will be relatively less elevated at the microburst time so it has a greater bp and is more likely to be detected. In other words, *bp* will be relatively larger for A_{1000} than A_{500}. This sensitivity manifests itself as a bias towards detecting narrower microbursts that we will address later in this study.

3.2 Microburst Fitting to Quantify Their Duration

We estimated the microburst duration using two methods that yielded similar results: the duration at half of the microburst's topographic prominence and duration from a Gaussian fit.

The topographic prominence is a simple and robust method to estimate the microburst duration used to identify curtains a similar-looking type of precipitation (Shumko et al., 2020). It is defined as the duration at half of the microburst topographic prominence: the height of the microburst relative to the maximum of the two minima on either side of the microburst peak. On each side of the microburst peak, the minima are searched for between the microburst and a higher peak on that side. While the topographic prominence method of estimating microburst durations is simple and robust, one of its downsides is its inability to automatically verify that the duration is representative of a single microburst. Therefore, we also fit microbursts with a Gaussian, and used the R^2 goodness of fit metric to filter out bad duration estimates.

The other method that we use to estimate the microburst duration is fitting a Gaussian shape to microbursts. The advantage of this method is that it allows us to evaluate the fit using a goodness of fit metric. By screening out bad fits, we exclude superposition of multiple microbursts that will unintentionally bias our microburst duration estimate.

We assumed a Gaussian superposed with a linear trend fit model. The Gaussian models the shape of the microburst; while the linear trend accounts for the electrons that are either trapped or quasi-trapped in the drift loss cone. The fit model is defined as:

$$c(t|A, t_0, \sigma, c_0, c_1) = Ae^{-\frac{(t-t_0)^2}{2\sigma^2}} + c_0 + c_1 t \tag{2}$$

where A, t_0, and σ are the Gaussian amplitude, center time, and standard deviation; while the c_0 and c_1 are the background count intercept and slope. The fit was applied over a number of data points determined by the maximum of either: 4x topographic prominence width or 0.5 seconds. A challenge to any robust and automated nonlinear regression algorithm is guessing the initial parameters. The initial parameter guesses for the Gaussian are provided by the topographic prominence and topographic duration estimates. The two linear trend initial parameters were: $c_0 = \text{median(counts)}$ and $c_1 = 0$. The optimal fit parameters were found using scipy's `curve_fit()` function in Python. We defined the microburst duration as the full width at half maximum (FWHM) of the microburst peak, defined as

$$\text{FWHM} = 2\sqrt{2\ln 2}\sigma. \tag{3}$$

To evaluate the fit, we used the R^2 goodness of fit metric. R^2 is defined as

$$R^2 = 1 - \frac{SS_{res}}{SS_{mean}} = 1 - \frac{\sum(c_i - f_i)^2}{\sum(c_i - \bar{c})^2} \tag{4}$$

where SS_{res} is the sum of the squared residuals between the observed counts c_i and the fit counts f_i for each time step, and likewise SS_{mean} is the sum of the squared residuals between c_i and the mean of the counts, $\bar{c}$.

One interpretation of R^2 is: fractionally how much better is the variance in the data explained by the model fit, compared to the null hypothesis horizontal line at $\bar{c}$. R^2 values vary from 1 when the fit perfectly describes the variance in the data, to $-\infty$ for poor fits (a fit can be much worse than the mean null hypothesis).

To account for overfitting that results from the variable number of data points used for each fit, the adjusted R^2, $\bar{R}^2$, was used. It is defined as

$$\bar{R}^2 = 1 - (1 - R^2)\frac{n-1}{n-p-1} \tag{5}$$

where n is the number of data points fit, and p is the number of parameters. Intuitively, $n-1$ is the number of degrees of freedom for the null hypothesis, and $n-p-1$ is the degrees of freedom for the fit model. Fits with $\bar{R}^2 > 0.9$ are considered good fits and

are used for the rest of this analysis. We compared the microburst duration estimated with the prominence and fit methods. With the $\bar{R}^2 > 0.9$ constraint, we found that for 85% of microbursts, the duration estimated by both methods agreed to within 25%.

Figure 1a shows an example of two superposed microbursts that had a fit $\bar{R}^2 = 0.83$ that were excluded from this study. On other hand, Fig. 1b-d show microbursts that were included in this study because the fit $\bar{R}^2 > 0.9$.

Lastly, Fig. 1c,d demonstrate the necessity of the linear fit to account for the changing background. The linear fit accounts for the non-zero mean background counts and the different amplitudes of the edges of the Gaussian. Of the 256,764 detected microbursts, 109,231 had $R^2 > 0.9$ and are used for the remainder of this study.

4 Results

We used the well-fit microbursts to quantify the distribution of microburst duration (FWHM) for all microbursts, as a function of the Auroral Electroject, and as a function of L and MLT. We begin with the overall microburst distribution.

Figure 2a shows the distribution of all well-fit microbursts. This distribution is peaked with the median at 98 ms and quickly drops off. The interquartile range spans about a factor of two in microburst duration, from 67 to 140 ms.

We then investigated the dependence of microburst duration as a function of geomagnetic activity. To be consistent with the prior wave and microburst studies, we use the AE index to quantify the level of geomagnetic disturbance. We adopt the same three AE intensity levels used in prior studies, such as Li, Thorne, Angelopoulos, Bortnik, et al. (2009), Douma et al. (2017), and Meredith et al. (2020): AE < 100, 100 < AE < 300, and AE > 300, in units of nanotesla. Figure 2b shows the distribution of microburst duration as a function of AE. This distribution is qualitatively similar: gradually narrowing and shifting to shorter durations with increasing AE. The median microburst duration decreases from 129 ms for 0 < AE < 100 to 94 ms for AE > 300.

Lastly, we investigated the duration distribution as a function of L and MLT. The joint distribution is shown in Fig. 3. Figure 3a-c show the 25%, 50%, and 75% percentiles of microburst durations in each L-MLT bin. The sparse bins with less than 100 well-fit microbursts are white. For reference, Fig. 3d shows the number of well-fit microbursts observed as a function of L and MLT.

Figure 3 shows that the microburst duration trend is almost identical for the different percentiles, so for simplicity we focus on the median distribution in Fig. 3b. In MLT, the median microburst duration increases by a factor of two: from 80 ms at midnight to 160 ms at noon. In L-shell, the median microburst duration slightly increases with L shell, most apparent near midnight MLT. To disentangle the L and MLT distribution, Fig. 4 shows the marginalized distributions; MLT was marginalized out in Fig. 4a and L-shell was marginalized out in Fig. 4b. Figure 4a shows a slight broadening of the microburst duration at higher L-shells; in contrast to Fig. 4b that clearly shows that the microburst duration increases from midnight to noon MLT.

5 Discussion and Conclusions

We first addressed the possible burst parameter bias to narrower microbursts. We used the microburst identification algorithm with three background values: A_{500}, A_{1000}, and A_{2000}. As described in section 3.1, a wider centered running average, A, will be more sensitive to wider and less prominent microbursts. Therefore, for wider A this bias manifests itself as a relative excess of longer duration microbursts. We identified a minor bias. The difference in the median microburst duration, using the microburst lists generated

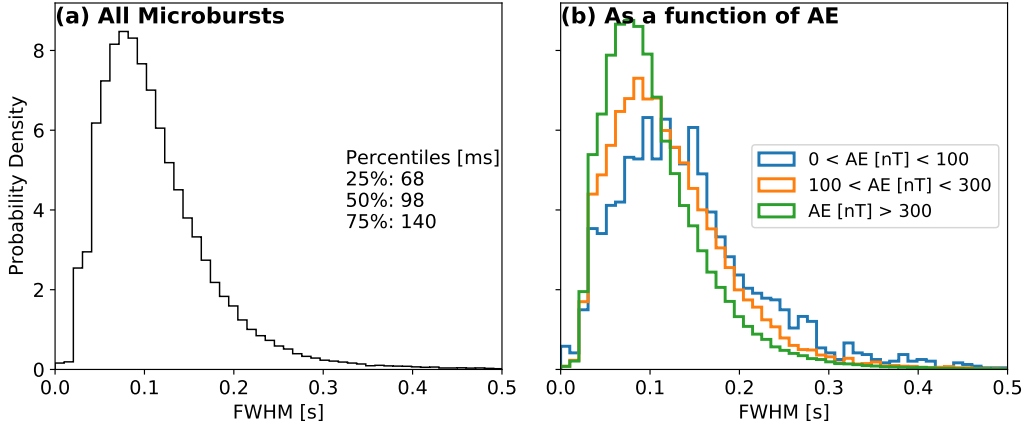Distribution of > 1 MeV Microburst Duration
SAMPEX/HILT

Figure 2. Panel a shows the distribution of all microburst full width at full maximum (FWHM). Panel b shows the distribution of all microbursts, categorized by the Auroral Electroject (AE) index into three bins: $0 < AE < 100$, $100 < AE < 300$, and $AE > 300$, in units of nanotesla. The median microburst duration is 129 ms for the $0 < AE < 100$ (2.4×10^3 microbursts), 110 ms for the $100 < AE < 300$ (1.8×10^4 microbursts), and 94 ms for the $AE > 300$ (9.3×10^4 microbursts) bins.

227   using A_{500} and A_{2000}, was 14 ms (corresponding to a 14% relative difference). Consid-
228   ering this bias and the distribution in Fig. 2a, we believe that the majority of > 1 MeV
229   microbursts have a true duration around 100 ms and the A_{500} is adequate to identify these
230   microbursts.

231   The microburst duration trend in L-shell is subtle; the 75th percentile of the du-
232   ration distribution, shown in in Fig. 3c, slightly increases at higher L-shells near mid-
233   night MLT. This is also noticeable in Fig. 4a. In contrast, the duration trend in MLT
234   is significant. The median microburst duration doubles from 80 to 160 ms between mid-
235   night and noon MLT. Now we will only focus on the MLT trend.

236   Chorus rising tone elements are believed to scatter microburst electrons (e.g. Bren-
237   eman et al., 2017; Saito et al., 2012; Miyoshi et al., 2020), thus we will compare the mi-
238   croburst duration trend in local time to the observed chorus trends. Two recent stud-
239   ies by Teng et al. (2017) and Shue et al. (2019) quantified the properties of equatorial
240   lower band (0.1-0.5 x electron gyrofrequency) chorus rising tone elements. Both stud-
241   ies found that the rising tone element duration distribution peaks at ≈ 250 ms around
242   midnight, and it broadens and shifts to ≈ 500 ms at noon MLT. Out of place because
243   here we're talking about the MLT distribution $\rightarrow$ Furthermore, (Teng et al., 2017) found
244   that the rising tone element duration distribution is broad and peaks at ≈ 500 ms when
245    $AE < 100$ nT and the distribution narrows and shifts to ≈ 250 ms for $AE > 300$ nT.
246   The chorus rising tone element trend in MLT scales by roughly the same factor of 2 as
247   the microburst duration trends we found in Fig 2b and 4b, but in general the chorus ris-
248   ing tone element duration is roughly 3 times longer than > 1 MeV microbursts. How-
249   ever, theory points to a different chorus property controlling the microburst duration.

250   Figure 4 in Chen et al. (2020) shows a test particle simulation result and the au-
251   thors describe what wave properties bound the microburst duration in time-energy space.
252   Medium energy ($\approx 50 - 300$ keV) microburst duration is controlled by the rising tone

Distribution of SAMPEX microburst durations in L-MLT

(a) 25th percentile

(b) 50th percentile

(c) 75th percentile
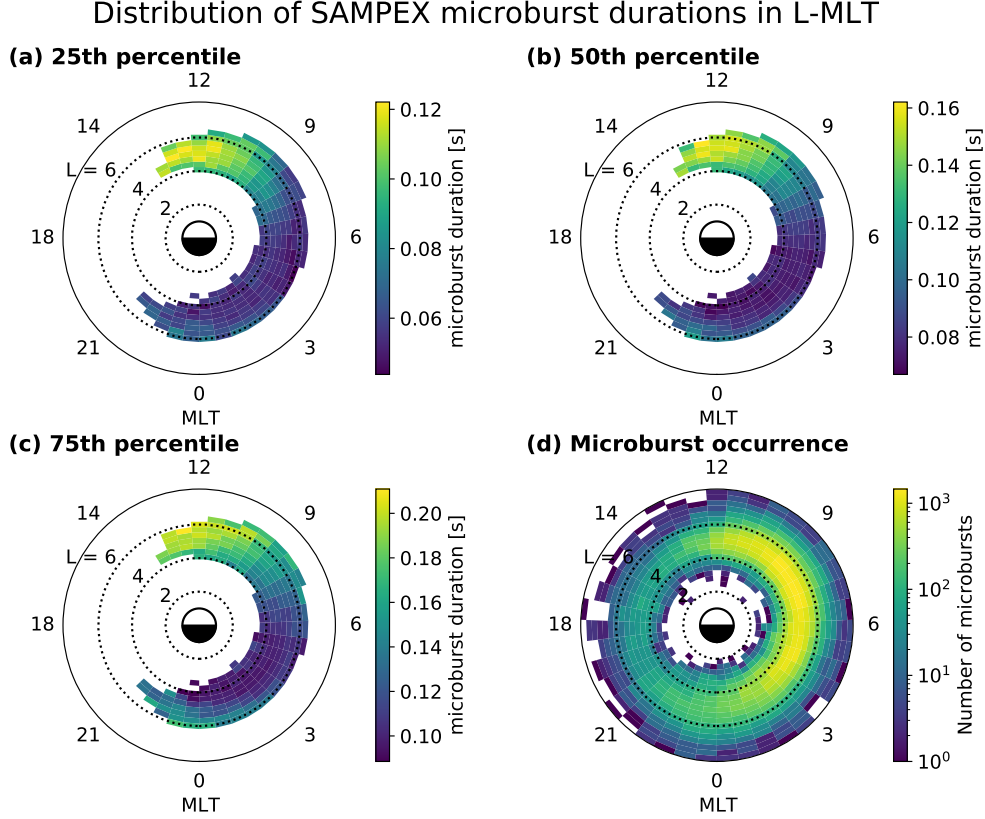
(d) Microburst occurrence

Figure 3. The joint distributions of microburst duration (FWHM) as a function of L and MLT. In each L-MLT bin with more than 100 good microburst fits, the 25th, 50th, and 75th percentiles of the duration were calculated and shown in panels a-c, respectively. The white bins in panels a-c have less than 100 good microburst fits. Panel d shows the distribution of the number of microbursts with 0 microbursts shown with the white bins.

Distribution of SAMPEX microburst durations in L and MLT
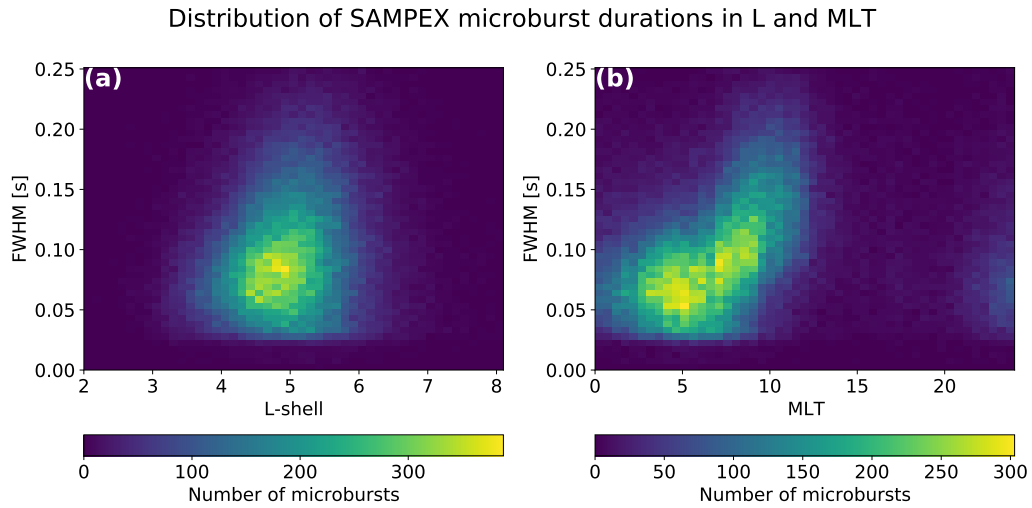
Figure 4. The marginalized distributions of the number of microbursts as a function of microburst duration (FWHM) and L shell in panel a and MLT in panel b.

element bandwidth. However, for higher energies the microburst duration is controlled by the wave's lower frequency and the upper magnetic latitude propagation. Comment that higher latitude chorus scatters higher energy electrons? What about Saito's time of flight model? While different model parameters may change what wave properties are responsible for scattering > 1 MeV microburst electrons, it is worth noting that Shue et al. (2019) found that the rising tone element bandwidth is qualitatively the same between midnight and noon MLT. The theory does not conclusively predict what chorus wave properties control the > 1 MeV microburst duration, and only the chorus rising tone duration shows a similar trend in MLT.

Check my arguments for clarity. High latitude chorus waves, found at $\approx 10 - 25$ degrees magnetic latitude off of the equator, can also play at important role at scattering microburst electrons (Lorentzen et al., 2001). Li, Thorne, Angelopoulos, Bortnik, et al. (2009) found that the majority of high latitude chorus waves are constrained to 6-12 MLT. Thus, it is tempting to conclude that the longer duration microbursts can be attributed to the low and high latitude chorus waves. However, because low latitude chorus waves are also observed at 0-12 MLT (Li, Thorne, Angelopoulos, Bortnik, et al., 2009), the resulting microburst duration distribution would reflect their superposition in the 6-12 MLT region. If low and high latitude chorus waves scattered microbursts with different durations, Fig. 4b would show the durations broaden or bifurcate from midnight to noon MLT. Because Fig. 4b shows the microburst duration only shift to longer durations, high vs low latitude chorus waves are an unlikely explanation for the microburst duration trend in MLT. Alex's comment: So I think here you're getting at the idea that the shape of the distributions isn't changing, and so you can get away with using median for all (25th/75th follow same progression). If you had a superposition of different populations then you might expect to see the different percentiles not move in lockstep if those percentiles allow you to cut out the different pops.

In summary, we found that the > 1 MeV microburst duration distribution is peaked at 100 ms, with 75% of microbursts narrower than 140 ms. We found no significant trend in the microburst duration as a function of L-shell, but we did find a strong trend as a function of MLT—the median microburst duration roughly doubles from 80 ms at midnight, to 160 ms at noon MLT. We found that the microburst duration trend in MLT scales similarly to the rising tone element duration, but the duration of rising tone elements is longer. Nonetheless, at this time modeling is not conclusive: the rising tone element duration is not predicted to control > 1 MeV microburst duration, but it predicts the bandwidth and/or the upper latitude of propagation.

References

Anderson, K. A., & Milton, D. W. (1964). Balloon observations of X rays in the auroral zone: 3. High time resolution studies. *Journal of Geophysical Research*, *69*(21), 4457–4479. Retrieved from `http://dx.doi.org/10.1029/JZ069i021p04457` doi: 10.1029/JZ069i021p04457

Baker, D. N., Mason, G. M., Figueroa, O., Colon, G., Watzin, J. G., & Aleman, R. M. (1993). An overview of the solar anomalous, and magnetospheric particle explorer (SAMPEX) mission. *IEEE Transactions on Geoscience and Remote Sensing*, *31*(3), 531–541.

Blake, J. B., Looper, M. D., Baker, D. N., Nakamura, R., Klecker, B., & Hovestadt, D. (1996). New high temporal and spatial resolution measurements by sampex of the precipitation of relativistic electrons. *Advances in Space Research*, *18*(8), 171 - 186. Retrieved from `http://www.sciencedirect.com/science/article/pii/0273117795009698` doi: http://dx.doi.org/10.1016/0273-1177(95)00969-8

Blum, L., Li, X., & Denton, M. (2015). Rapid MeV electron precipitation as observed by SAMPEX/HILT during high-speed stream-driven storms. *Journal of Geophysical Research: Space Physics*, *120*(5), 3783–3794. Retrieved from `http://dx.doi.org/10.1002/2014JA020633` (2014JA020633) doi: 10.1002/2014JA020633

Breneman, A., Crew, A., Sample, J., Klumpar, D., Johnson, A., Agapitov, O., ... others (2017). Observations directly linking relativistic electron microbursts to whistler mode chorus: Van allen probes and FIREBIRD II. *Geophysical Research Letters*.

Chen, L., Breneman, A. W., Xia, Z., & Zhang, X.-j. (2020). Modeling of bouncing electron microbursts induced by ducted chorus waves. *Geophysical Research Letters*, *47*(17), e2020GL089400. Retrieved from `https://agupubs.onlinelibrary.wiley.com/doi/abs/10.1029/2020GL089400` (e2020GL089400 10.1029/2020GL089400) doi: https://doi.org/10.1029/2020GL089400

Crew, A. B., Spence, H. E., Blake, J. B., Klumpar, D. M., Larsen, B. A., O'Brien, T. P., ... Widholm, M. (2016). First multipoint in situ observations of electron microbursts: Initial results from the NSF FIREBIRD II mission. *Journal of Geophysical Research: Space Physics*, *121*(6), 5272–5283. Retrieved from `http://dx.doi.org/10.1002/2016JA022485` (2016JA022485) doi: 10.1002/2016JA022485

Datta, S., Skoug, R., McCarthy, M., & Parks, G. (1997). Modeling of microburst electron precipitation using pitch angle diffusion theory. *Journal of Geophysical Research: Space Physics*, *102*(A8), 17325–17333.

Douma, E., Rodger, C., Blum, L., O'Brien, T., Clilverd, M., & Blake, J. (2019). Characteristics of relativistic microburst intensity from sampex observations. *Journal of Geophysical Research: Space Physics*.

Douma, E., Rodger, C. J., Blum, L. W., & Clilverd, M. A. (2017). Occurrence characteristics of relativistic electron microbursts from SAMPEX observations. *Journal of Geophysical Research: Space Physics*, *122*(8), 8096–8107. Retrieved from `http://dx.doi.org/10.1002/2017JA024067` (2017JA024067) doi: 10.1002/2017JA024067

Horne, R. B., & Thorne, R. M. (2003). Relativistic electron acceleration and precipitation during resonant interactions with whistler-mode chorus. *Geophysical Research Letters*, *30*(10). Retrieved from `http://dx.doi.org/10.1029/2003GL016973` (1527) doi: 10.1029/2003GL016973

Johnson, A., Shumko, M., Griffith, B., Klumpar, D., Sample, J., Springer, L., ... others (2020). The FIREBIRD-II CubeSat mission: Focused investigations of relativistic electron burst intensity, range, and dynamics. *Review of Scientific Instruments*, *91*(3), 034503.

Klecker, B., Hovestadt, D., Scholer, M., Arbinger, H., Ertl, M., Kastele, H., ... others (1993). HILT: A heavy ion large area proportional counter telescope for solar and anomalous cosmic rays. *IEEE transactions on geoscience and remote sensing*, *31*(3), 542–548.

Kurita, S., Miyoshi, Y., Blake, J. B., Reeves, G. D., & Kletzing, C. A. (2016). Rel-

ativistic electron microbursts and variations in trapped mev electron fluxes during the 8–9 october 2012 storm: Sampex and van allen probes observations. *Geophysical Research Letters*, *43*(7), 3017-3025. Retrieved from `https://agupubs.onlinelibrary.wiley.com/doi/abs/10.1002/2016GL068260` doi: https://doi.org/10.1002/2016GL068260

Li, W., Thorne, R., Angelopoulos, V., Bonnell, J., McFadden, J., Carlson, C., ... Auster, H. (2009). Evaluation of whistler-mode chorus intensification on the nightside during an injection event observed on the THEMIS spacecraft. *Journal of Geophysical Research: Space Physics*, *114*(A1).

Li, W., Thorne, R. M., Angelopoulos, V., Bortnik, J., Cully, C. M., Ni, B., ... Magnes, W. (2009). Global distribution of whistler-mode chorus waves observed on the THEMIS spacecraft. *Geophysical Research Letters*, *36*(9). Retrieved from `http://dx.doi.org/10.1029/2009GL037595` (L09104) doi: 10.1029/2009GL037595

Lorentzen, K. R., Blake, J. B., Inan, U. S., & Bortnik, J. (2001). Observations of relativistic electron microbursts in association with VLF chorus. *Journal of Geophysical Research: Space Physics*, *106*(A4), 6017–6027. Retrieved from `http://dx.doi.org/10.1029/2000JA003018` doi: 10.1029/2000JA003018

Meredith, N. P., Horne, R. B., Shen, X.-C., Li, W., & Bortnik, J. (2020). Global model of whistler mode chorus in the near-equatorial region ($|\lambda_m| < 18°$). *Geophysical Research Letters*, *47*(11), e2020GL087311.

Miyoshi, Y., Saito, S., Kurita, S., Asamura, K., Hosokawa, K., Sakanoi, T., ... others (2020). Relativistic electron microbursts as high energy tail of pulsating aurora electrons.

Nakamura, R., Isowa, M., Kamide, Y., Baker, D., Blake, J., & Looper, M. (2000). Observations of relativistic electron microbursts in association with VLF chorus. *J. Geophys. Res*, *105*, 15875–15885.

O'Brien, T. P., Looper, M. D., & Blake, J. B. (2004). Quantification of relativistic electron microburst losses during the GEM storms. *Geophysical Research Letters*, *31*(4). Retrieved from `http://dx.doi.org/10.1029/2003GL018621` (L04802) doi: 10.1029/2003GL018621

O'Brien, T. P., Lorentzen, K. R., Mann, I. R., Meredith, N. P., Blake, J. B., Fennell, J. F., ... Anderson, R. R. (2003). Energization of relativistic electrons in the presence of ULF power and MeV microbursts: Evidence for dual ULF and VLF acceleration. *Journal of Geophysical Research: Space Physics*, *108*(A8). Retrieved from `http://dx.doi.org/10.1029/2002JA009784` doi: 10.1029/2002JA009784

Saito, S., Miyoshi, Y., & Seki, K. (2012). Relativistic electron microbursts associated with whistler chorus rising tone elements: Gemsis-rbw simulations. *Journal of Geophysical Research: Space Physics*, *117*(A10), n/a–n/a. Retrieved from `http://dx.doi.org/10.1029/2012JA018020` (A10206) doi: 10.1029/2012JA018020

Seppälä, A., Douma, E., Rodger, C., Verronen, P., Clilverd, M. A., & Bortnik, J. (2018). Relativistic electron microburst events: Modeling the atmospheric impact. *Geophysical Research Letters*, *45*(2), 1141–1147.

Shue, J.-H., Nariyuki, Y., Katoh, Y., Saito, S., Kasahara, Y., Hsieh, Y.-K., ... Goto, Y. (2019). A systematic study in characteristics of lower band rising-tone chorus elements. *Journal of Geophysical Research: Space Physics*, *124*(11), 9003–9016.

Shumko, M., Johnson, A. T., O'Brien, T. P., Turner, D. L., Greeley, A. D., Sample, J. G., ... Halford, A. J. (2020). Statistical properties of electron curtain precipitation estimated with aerocube-6. *Journal of Geophysical Research: Space Physics*, *125*(12), e2020JA028462. Retrieved from `https://agupubs.onlinelibrary.wiley.com/doi/abs/10.1029/2020JA028462` (e2020JA028462 10.1029/2020JA028462) doi: https://doi.org/10.1029/

2020JA028462

Shumko, M., Turner, D. L., O'Brien, T. P., Claudepierre, S. G., Sample, J., Hartley, D. P., ... Mitchell, D. G. (2018). Evidence of microbursts observed near the equatorial plane in the outer van allen radiation belt. *Geophysical Research Letters*, *45*(16), 8044-8053. Retrieved from `https://agupubs.onlinelibrary.wiley.com/doi/abs/10.1029/2018GL078451` doi: 10.1029/2018GL078451

Summers, D. (2005). Quasi-linear diffusion coefficients for field-aligned electromagnetic waves with applications to the magnetosphere. *Journal of Geophysical Research: Space Physics*, *110*(A8), n/a–n/a. Retrieved from `http://dx.doi.org/10.1029/2005JA011159` (A08213) doi: 10.1029/2005JA011159

Teng, S., Tao, X., Xie, Y., Zonca, F., Chen, L., Fang, W., & Wang, S. (2017). Analysis of the duration of rising tone chorus elements. *Geophysical Research Letters*, *44*(24), 12–074.

Thébault, E., Finlay, C. C., Beggan, C. D., Alken, P., Aubert, J., Barrois, O., ... others (2015). International geomagnetic reference field: the 12th generation. *Earth, Planets and Space*, *67*(1), 79.

Thorne, R. M. (2010). Radiation belt dynamics: The importance of wave-particle interactions. *Geophysical Research Letters*, *37*(22). Retrieved from `http://dx.doi.org/10.1029/2010GL044990` (L22107) doi: 10.1029/2010GL044990

Thorne, R. M., O'Brien, T. P., Shprits, Y. Y., Summers, D., & Horne, R. B. (2005). Timescale for MeV electron microburst loss during geomagnetic storms. *Journal of Geophysical Research: Space Physics*, *110*(A9). Retrieved from `http://dx.doi.org/10.1029/2004JA010882` (A09202) doi: 10.1029/2004JA010882